JOURNAL OF SPACECRAFT AND ROCKETS
Vol. 29, No. 4, July–August 1992

# Medium Energy Ion Mass and Neutral Atom Spectrometer

H. D. Voss,* E. Hertzberg,† A. G. Ghielmetti,‡ S. J. Battel,§ K. L. Appert,† B. R. Higgins,†
D. O. Murray,* and R. R. Vondrak¶
*Lockheed Palo Alto Research Laboratory, Palo Alto, California 94304*

**The primary objective of the medium energy ion mass spectrometer (ONR 307-8-3) on the CRRES is to obtain the necessary data to construct models of the energetic ion (10–2000 keV-amu/$q^2$) and neutral atom (10–1500 keV) environment of the Earth's radiation belts. The spectrometer measures the energetic ion composition, energy spectrum, charge, and pitch angle distribution with good mass, temporal, and spatial resolution. The ion rejection in the neutral detector is <100 MeV-amu/$q^2$. The instrument principle of operation is based on ion momentum separation in a 7000-G magnetic field followed by energy and mass defect analysis using an array of cooled silicon solid-state detectors. The architecture is parallel with simultaneous mass and energy analysis at relatively high sensitivity (100% duty cycle). The instrument performed as designed in orbit with the major groups of hydrogen, helium, oxygen, and neutrals clearly resolved. The energetic ion composition during the August 26, 1990, storm illustrates the instrument performance.**

## I. Introduction

THE medium energy ion mass spectrometer (IMS-HI) on the Combined Release and Radiation Effects satellite (CRRES) measures the energy spectra and pitch angle distributions of magnetospheric ions and neutral particles. The instrument is designed specifically to measure the highly variable fluxes of ions in the energy range from a few tens of kiloelectron volts to a few hundred kiloelectron volts that populate the ring current and produce the variations seen in the magnetic Dst index associated with magnetic storms.

Ring-current studies based on data from the Explorer 45 spacecraft[1] were hampered because the detectors did not distinguish between protons and higher mass ions. Other researchers[2–5] have demonstrated the importance of including neutrals and ions other than protons to explain the decay rates observed in the ring current. By charge exchange with thermal hydrogen atoms, energetic ions become neutrals and can escape from the Earth's environment. This is a significant loss process for the medium-energy ring current ions. More recent measurements obtained by the medium-energy plasma analyzer on the AMPTE/CCE spacecraft have demonstrated the advantages of comprehensive ion composition measurements for the study of ring current processes.[6]

On CRRES, ring-current ion composition and neutral atom measurements are provided in part by the IMS-HI instrument. This instrument is one of four instruments that comprise the Office of Naval Research (ONR-307) energetic particles and ion compositon (EPIC) experiment. The contiguous mapping of the particle distribution over the radial distance range from 400 km to 5.5 Earth radii (Re) near the equatorial plane provides a comprehensive data base that can be used for studies of radiation belt and ring-current energization, injection, and loss processes.

Received July 12, 1991; revision received Oct. 11, 1991; accepted for publication Oct. 11, 1991. 

*Staff Scientist, Space Sciences Laboratory, Dept. 91-20, B/255, 3251 Hanover Street.

†Research Engineer, Space Sciences Laboratory, Dept. 91-20, B/255, 3251 Hanover Street.

‡Research Scientist, Space Sciences Laboratory, Dept. 91-20, B/255, 3251 Hanover Street.

§Space Sciences Laboratory, Dept. 91-20, B/255, 3251 Hanover Street; currently, Consultant, Battel Engineering. Member AIAA.

¶Manager, Space Sciences Laboratory, Dept. 91-20, B/255, 3251 Hanover Street. Associate Fellow AIAA.

## II. Measuring Techniques

The IMS-HI instrument is based on ion momentum separation in a magnetic field followed by energy and mass defect analysis using an array of cooled silicon solid-state sensors as shown in Fig. 1. The entrance collimator consists of a series of rectangular baffles that define the ion beam angular resolution and a broom magnet to reject electrons with energy less than 1 MeV.

After exiting the collimator ions enter a 7000-G magnetic field where they are deflected (mv/qB) onto a set of six passively cooled (−50°C) silicon surface-barrier detectors. The technique of cooling solid-state detectors for high-resolution [<2 keV full width at half maximum (FWHM)] energetic ion measurements in spacecraft instruments was discussed by Voss et al.[7] and was successfully demonstrated in the stimulated emission of energetic particles (SEEP) experiment on the S81-1 satellite.[8] The energy range covered varies with ion species and is approximately em/$q^2$ = 10–2000 keV-amu/$q^2$. A seventh sensor, located directly in line with the collimator, measures energetic neutrals and has an ion rejection of approx-

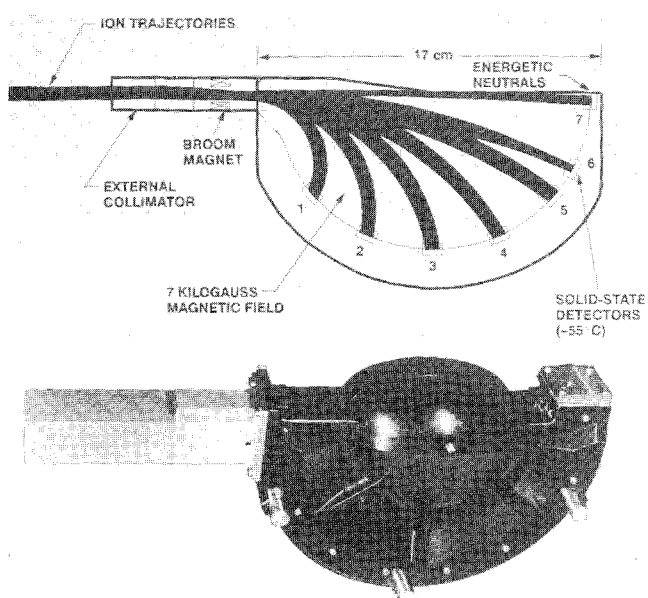


**Fig. 1 Principle of operation for IMS-HI is based on ion momentum, mass defect, and energy analysis using an array of cooled solid-state detectors. Magnet is shown in the upper portion of the figure and the ion optics in the lower portion.**

**Table 1 Medium energy ion mass spectrometer (IMS-HI) specifications**

| | |
|---|---|
| Analyzer | 7 kg magnet ($m/q^2$) and mass defect |
| Sensors | Silicon surface barrier (−55°C) |
| Number of imaging sensors | 7 at 0.5 $cm^2$ each |
| Look direction from spin axis | 75 deg |
| Particles and energy range: | |
| Neutrals | 10–1500 keV |
| Protons | 15–2000 keV |
| Helium | 4–500 keV |
| Oxygen | 20–130 keV |
| Oxygen + + | 20–500 keV |
| Other ions | E>20 keV |
| Number of differential mass channels | 64 |
| Number of high rate mass channels | 4 |
| Number of differential energy channels | 6 |
| Pitch angle resolution | 4 deg FWHM |
| Geometrical factor | $10^{-2}$–$10^{-3}$ $cm^2sr$ |
| Duty cycle | 100% |

imately 100 MeV-amu/$q^2$. Detailed instrument specifications are given in Table 1.

The instrument features simultaneous mass and energy analysis at relatively large geometrical factors ($10^{-3}$ to $10^{-2}$ $cm^2$ sr). Simultaneous measurements of charge states can be identified for each $m/q^2$ and for the same $m/q^2$, in some cases, within the solid-state detector due to dead zone and mass defect energy losses for equal $m/q^2$ (e.g., $O^{++}$ and $He^+$). Because of the multisensor design and parallel processing electronics, the dynamic range in flux covered is approximately six orders of magnitude.

A simulation of the ion separation in a 7000-G magnetic field is shown in the position-energy diagram of Fig. 2. The image surface $S$ is defined as the arc length, beginning at the collimator, for a radius $R = 8$ cm. Solid-state detectors 1–7 are located at angles Θ of 40, 65, 90, 115, 140, 162.5, and 180 deg, respectively. Solid-state detectors 1–6 are $n$-type silicon having either 20 or 40 $\mu g\ cm^{-2}$ of gold surface deposit. The neutral detector is of $p$-type silicon to improve light rejection and radiation damage sensitivity and has 20 $\mu g\ cm^{-2}$ of aluminum surface deposit. The energy loss in surface-barrier windows for H, He, and O is discussed by Voss.[9] The mass defect in solid-state detectors results from energy loss of nonionizing nuclear collisions within the solid that reduce the efficiency of electronic signal generation. The mass defect increases with atomic weight of the nuclei in a well-understood way[10] and causes further mass separation, with commensurate energy scatter, for the heavier nuclei.

The magnet section consists of a yoke, pole pieces, and a SmCo permanent magnet. To produce a homogeneous magnetic field with high inducton ( ~ 7 kG) in a 5-mm gap and with minimized weight, the best available magnetic material (SmCo Recoma 25, with 25 MGOe energy product) was selected. The yoke completely surrounds the magnetic field except for the entrance aperture, permitting one to reduce the magnetic resistivity in the return flux section and to minimize the magnetic stray fields. Shape and dimensions of the yoke are optimized to reduce weight and are designed for a uniform magnetic induction of 19 kG anywhere within the yoke. The resultant complex shape necessitates the use of numerical computer-aided machining methods to meet the weight requirement and design goal of $\lesssim 100$ nT magnetic stray field at a distance of 1 m. A yoke material (Hyperco 50) that possesses relatively high permeability (2000–4000) at high-induction levels (20 kG) was chosen. The mass of the flight yoke and magnet assembly is about 5.7 kg.

A functional system diagram of the IMS-HI is shown in Fig. 3. Variable pulse-height signals from the ion sensors are each routed for analysis to a peak detector circuit and analog multiplexer. Each peak detector circuit is allowed to track and hold the highest peak value for input pulses below the programmable low level threshold $V_T$ and to hold and stop sampling for input pulses above $V_T$. This allows signals to be processed well into the noise level for added in-orbit performance. The sample interval for each detector is 45 $\mu s$. The read and reset of each peak detector circuit is controlled by strobes from a master clock so that a continuous and sequential scan is made of each detector.

Simultaneous with the reset command, a 256-channel analog-to-digital converter is activated, and the resulting digital pulse height (8 bits) is placed on the address bus of an energy lookup table. Also placed on the address bus of this RAM are the 3 bits that specify which detector is being processed. The content of this memory cell (16 bits) is read into an accumulator, incremented by one, and then read back into the memory cell. An address counter is then used to sequentially step through the entire RAM for telemetry readout. A data compressor packs the 16-bit sum into an 8-bit byte for serial interface with the satellite telemetry.

The instrument operates in two basic modes; mass lock and mass scan. In the mass scan mode, each of the seven solid-state sensors is pulse-height analyzed into 256 levels of which 64 intervals are accumulated in memory and read out every 8 s. This mode is used to scan all mass peaks within the range of the sensor relative to the background continuum. In the mass lock mode, each of the seven solid-state sensors is pulse-height analyzed into 256 levels, of which four intervals (typically, four ions) are accumulated in memory and read out every half-second. This mode is used for making rapid spectral snapshots of four ions as a function of pitch angle. Baseline operation of the instrument will be to toggle every 32.768 s between the mass lock mode and the mass scan mode.

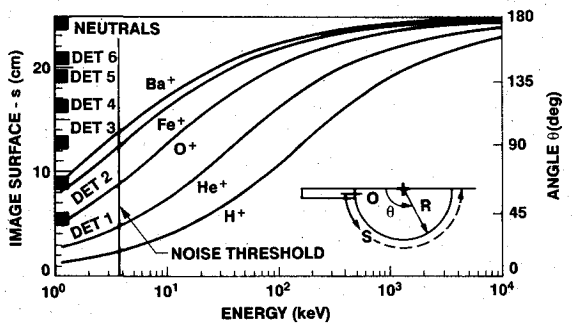


**Fig. 2 Energy of various ions that are mapped onto the detector focal surface $S$ is shown for a 7000-G magnetic field.**

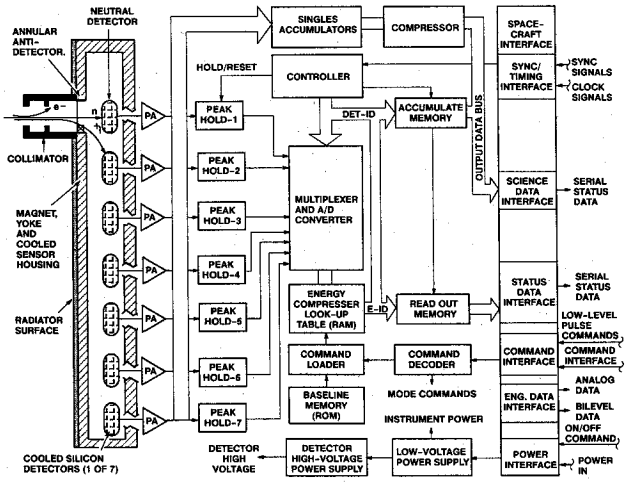


**Fig. 3 Functional block diagram of the IMS-HI instrument.**

## III. Calibration

The IMS-HI instrument was calibrated at Goddard Space Flight Center (GSFC) using the low-energy accelerator for ions up to 150 keV. The instrument was mounted on a scan platform in a vacuum chamber at the output end of the accelerator beam line. At a bend in the beam line, an electromagnet was used to select the desired mass after the electrostatic acceleration. A solid-state detector at the entrance to the vacuum test chamber was used to monitor the beam stability. The instrument was calibrated using $H^+$, $He^+$, $He^{++}$, $N^+$, $N^{++}$, $O^+$, and $O^{++}$ ions. The neutral detector was calibrated using energetic neutral hydrogen atoms.

To illustrate the instrument performance during calibration, an energy scan for protons impinging on detector 2 is shown in Fig. 4. The calibration data are currently being compared to the instrument computer model and to the flight data to arrive at the best-fit calibrations. The energy passbands are very clean as indicated in Fig. 4 and scattering from the pole pieces is less than 0.2%. The background rate can be subtracted using an algorithm based on the differential pulse-height spectrum in each of the seven detectors and the omnidirectional megaelectron volt electron flux.

In addition to the accelerator calibrations, the instrument was tested with radioactive sources at $-30°C$ in its final flight configuration. Six T1-204 sources of varying intensities were used to saturate the sensors in a known fashion to calibrate flux rate effects. An internal electronic pulser was also included in the instrument to give several pulse heights at the detector front end to calibrate gain, linearity, and resolution in orbit. It has also been observed in orbit that, when the instrument is illuminated with high fluxes of megaelectron volt electrons in the outer belt, K-alpha lines are present and associated with high-atomic-number materials near the sensors.

## IV. Preliminary Flight Results

The instrument design temperatures were achieved: $-55°C$ for the magnet and sensors, $-12°$ C for the preamps, and 0°C for the electronics box. The sensors' noise thresholds were therefore well within specifications. This is shown in Fig. 5 for detector 1 during orbit 77. Here the primary hydrogen peak is at 18 keV with a noise threshold of about 4 keV and a noise resolution of about 2 keV FWHM.

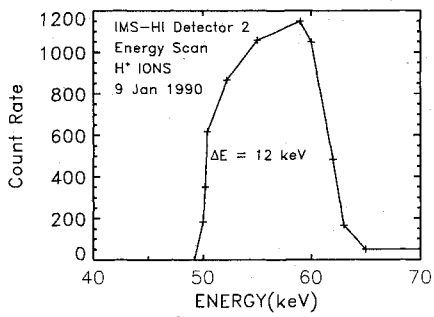


**Fig. 4 Energy passband for protons in detector 2 obtained during preflight calibrations.**

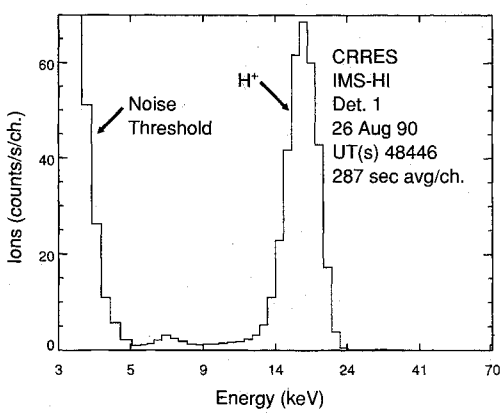


**In-flight data from detector 1 indicates a noise threshold of 4 keV and a hydrogen ion peak resolution of 2 keV FWHM.**

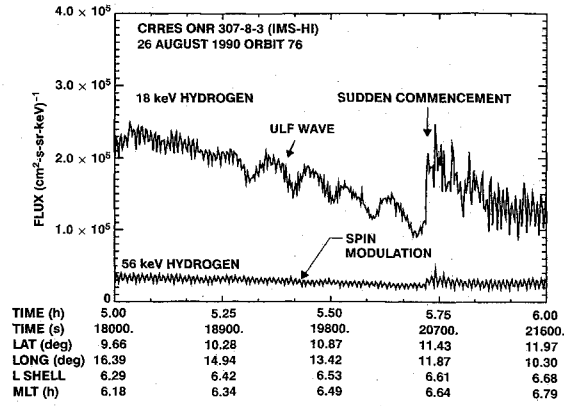


**Fig. 6 Example of scalar data from detector 1 and 2 for protons during the August 26, 1990, sudden commencement.**

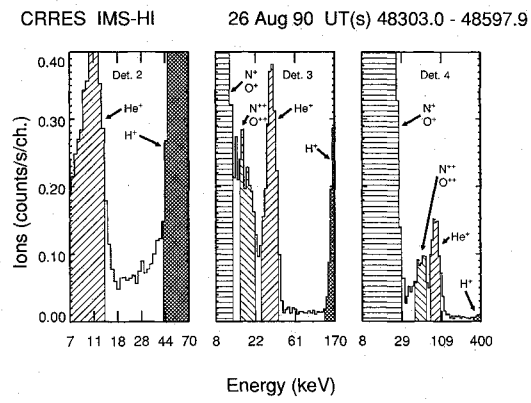


**Fig. 7 Ion mass peaks observed in detectors 2, 3, and 4 during the August 26, 1990, storm.**

The scalar data for 18- and 56-keV protons during the sudden commencement on August 26, 1990, is illustrated in Fig. 6. The major ultra lower frequency (ULF) wave-particle interaction is at 18 keV and nearly absent at 56 keV.

The final example of instrument performance is shown in Fig. 7 for the 64-channel mass spectrum of detectors 2, 3, and 4. These data were obtained on August 26, 1990 over a 5-min interval near $L = 5.0$. The distributions shown are for the raw count rates and do not have noise filtering, efficiencies, and other corrections included. The energy scale is preliminary and represents the deposited energy of the ions in the solid-state detectors.

The $H^+$ and $He^+$ peaks are conspicuous in each of the detectors as noted. The importance of mass defect in the solid-state detector is illustrated well in detector 4 for $He^+$ and $O^{++}$. Both ions have the same $m/q^2$ and thus the same energy incident on the detector (95 keV). Because the oxygen ion is less efficient at generating electron hole pairs, its peak is shifted down from the $He^+$ peak by about 30 keV. It is well separated from the $He^+$ and $N^+/O^+$ peaks. Thus, over certain energy and mass intervals the mass defect is an effective method of separating ion beams in a magnetic spectrometer. To obtain the ion flux, the penetrating backgrounds and skirts of the strong ion peaks must be properly subtracted using peak-analysis software.

## V. Summary

The IMS-HI experiment on CRRES operated successfully since launch. Preliminary results show that the instrument is

able to distinguish all of the major ion species and a few minor species with good time resolution. These measurements will comprise an important data base for studies of radiation belt and ring-current energization, injection, and decay rates.

## Acknowledgments

This effort was supported by the Office of Naval Research under Contract N00014-83-C-0476 and by the Lockheed Independent Research Program. The authors wish to thank F. Hilsenrath, L. A. Hooker, T. C. Sanders, D. A. Simpson, and V. F. Waltz for their efforts in the design, development, and fabrication of this instrument. We wish to thank R. M. Robinson and J. Mobilia for comments on the manuscript, and R. A. Baraze and R. McDonald for their efforts in data analysis. Appreciation is extended to R. G. Joiner for his program management role of our instruments at ONR. We also deeply appreciate the assistance of W. L. Imhof, J. M. Quinn, J. B. Reagan, R. D. Sharp, and E. G. Shelley. The assistance of S. Brown of GSFC was critical to the final calibration of this instrument.

## References

[1]Smith, P. H., and Hoffman, R. A., "Ring Current Particle Distributions During the Magnetic Storms of December 16–18, 1971," *Journal of Geophysical Research,* Vol. 78, No. 22, 1973, pp. 4731–4737.

[2]Lyons, L. R., and Evans, D. S., "The Inconsistency Between Proton Charge Exchange and the Observed Ring Current Decay," *Journal of Geophysical Research,* Vol. 81, No. 34, 1976, pp. 6197–6200.

[3]Spjeldvik, W. N., and Fritz, T. A., "Energetic Ionized Helium in the Quiet Time Radiation Belts: Theory and Comparison with Observations," *Journal of Geophysical Research,* Vol. 83, No. A2, 1978, pp. 654–662.

[4]Tinsley, B. A., "Effects of Charge Exchange Involving H and $H^+$ in the Upper Atmosphere," *Planetary and Space Science,* Vol. 26, 1978, p. 847.

[5]Williams, D. J., "Dynamics of the Earth's Ring Current: Theory and Observation," *Space Science Review,* Vol. 42, 1985, p. 375.

[6]McEntire, R. W., Lui, A. T. Y., Krimigis, S. M., and Keath, E. P., "AMPTE/CCE Energetic Particle Composition Measurements During the September 4, 1984 Magnetic Storm," *Geophysical Research Letters,* Vol. 12, No. 5, 1985, pp. 317–320.

[7]Voss, H. D., Reagan, J. B., Imhof, W. L., Murray, D. O., Simpson, D. A., Cauffman, D. P., and Bakke, J. C., "Low Temperature Characteristics of Solid State Detectors for Energetic X-ray, Ion and Electron Spectrometers," *IEEE Transactions on Nuclear Science,* Vol. NS-29, 1982, pp. 164–168.

[8]Imhof, W. L., Reagan, J. B., Voss, H. D., Gaines, E. E., Datlowe, D. W., Mobilia, J., Helliwell, R. A., Inan, U. S., Katsufrakis, J., and Joiner, R. G., "The Modulated Precipitation of Radiation Belt Electrons by Controlled Signals from VLF Transmitters," *Geophysical Research Letters,* Vol. 10, No. 8, 1983, pp. 615–618.

[9]Voss, H. D., "Energy and Primary Mass Determination Using Multiple Solid State Detectors," *IEEE Transactions on Nuclear Science,* Vol. NS-29, 1982, pp. 178–181.

[10]Forcinal, G., Siffert, P., and Coche, A., "Pulse Height Defects due to Nuclear Collisions Measured with Thin Window Silicon Surface Barrier Detector," *IEEE Transactions on Nuclear Science,* Vol. NS-15, 1968, p. 475.